Inorganic Chemistry

Article

pubs.acs.org/IC

A Series of Weak Ferromagnets Based on a Chromium–Acetylide–TTF Type Complex: Correlation of the Structures and Magnetic Properties and Origin of the Weak Ferromagnetism

Junichi Nishijo*[,†,‡] and Masaya Enomoto[§]

[†]Department of Interdisciplinary Science and Engineering, Meisei University, 2-1-1 Hodokubo, Hino, Tokyo 191-8506, Japan

[‡]Institute for Molecular Science, National Institutes of Natural Sciences and The Graduate University for Advanced Studies, Myodaiji, Nishigo-naka 38, Okazaki, Aichi 444-8585, Japan

[§]Department of Chemical Science and Technology, Graduate School of Chemical Science and Technology, Tokyo University of Science, Kagurazaka 1-3, Shinjuku-ku, Tokyo 162-8601, Japan

Supporting Information

ABSTRACT: The crystal structures and magnetic properties of a series of new weak ferromagnets containing a chromium–acetylide–tetrathiafulvalene (TTF) type complex, [CrCyclam(C≡C-5-methyl-4′5′-ethylenedithio-TTF)$_2$]$^{2+}$ ([**1**]$^{2+}$), were investigated. The six new isostructural weak ferromagnets [**1**][BF_4]$_2$(PhF)$_2$(MeCN), [**1**][ClO_4]$_2$(PhF)$_2$(MeCN), [**1**][ReO_4]$_2$(PhCl)$_2$(MeCN), [**1**][ClO_4]$_2$(PhBr)$_3$, [**1**][ReO_4]$_2$(PhBr)$_3$, and [**1**][ClO_4]$_2$(PhI)$_3$ contain ferrimagnetic chain structures of [**1**]$^{2+}_\infty$ with different interchain distances that are dependent on the sizes of the anions and solvent molecules. Magnetic measurements of the salts revealed that the weak ferromagnetic transition temperature gradually increases from 14.5 to 26.0 K as the interchain distance decreases from 3.997(2) to 3.803(2) Å, while the remanent magnetization at 2 K decreases from 0.0215 to 0.0079 μ_B. The observed magnetic properties and crystal structures suggest that the weak ferromagnetism originates from the single-ion anisotropy of [**1**]$^{2+}$, where a stronger interchain antiferromagnetic interaction not only causes a higher transition temperature but also suppresses the noncollinear canted spin alignment.

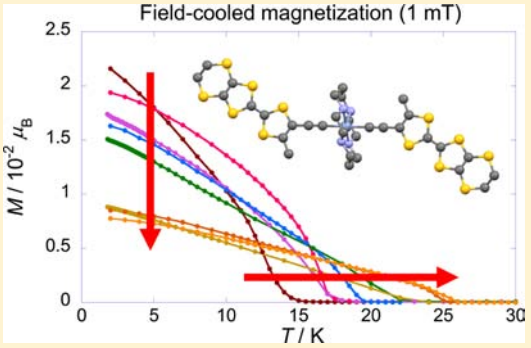

INTRODUCTION

There has been considerable interest in transition-metal complexes with redox-active ligands that exhibit unique features such as excellent catalytic activity,[1] electrochemically switchable luminescence,[2] and electrochemically controlled magnetism.[3] Among the many redox-active ligands, tetrathiafulvalene (TTF) derivatives have attracted much attention in recent decades[4] due to their outstanding features. First, most TTF derivatives are quite stable in both neutral and cation radical states. Second, because procedures for the synthesis of TTF derivatives are well established,[5] various TTF-type ligands with desired functional groups are available. Third, TTF derivatives are useful in constructing strong intermolecular interactions due to their planar molecular shape and vertically oriented π orbital, which enables a large intermolecular orbital overlap. For instance, the strength of the spin–spin exchange interaction $2|J|/k_B$ between π-stacked TTF radicals can become stronger than 300 K,[6] where k_B is the Boltzmann constant and J is defined in the following Hamiltonian

$$H = -2J \sum_i S_i S_{i+1} \cdot \quad (1)$$

These superior features of TTF derivatives have realized outstanding materials, including redox-active cage structures,[7] solid-state solvatochromic materials,[8] photoluminescent materials,[9] molecule-based magnets,[10] and multifunctional materials.[11]

Recently, the author and co-workers reported a new transition-metal–TTF type complex, [Cr^{III}Cyclam(C≡C-5-methyl-4′5′-ethylenedithio-TTF)$_2$]$^+$ ([**1**]$^+$, Cyclam = 1,4,8,11-tetraazacyclotetradecane; Figure 1),[12] the electrochemical oxidation of which in a solution of [ClO_4]$^-$ or [BF_4]$^-$ in an

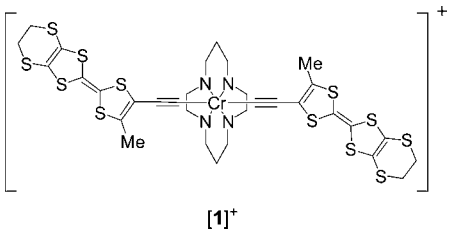

[**1**]$^+$

Figure 1. Molecular structure of [**1**]$^+$.

Received: August 30, 2013
Published: October 25, 2013

Table 1. Crystal Data and Structure Refinement Details

	[**1**][BF_4]$_2$(PhF)$_2$(MeCN)	[**1**][ClO_4]$_2$(PhF)$_2$(MeCN)	[**1**][ClO_4]$_2$($PhBr$)$_3$	[**1**][ClO_4]$_2$(PhI)$_3$	[**1**][ReO_4]$_2$(PhCl)$_2$(MeCN)	[**1**][ReO_4]$_2$($PhBr$)$_3$
chem formula	$C_{46}H_{51}B_2CrF_{10}N_5S_{12}$	$C_{46}H_{51}C_{12}CrF_2N_5O_8S_{12}$	$C_{50}H_{53}Br_3Cl_2CrN_4O_8S_{12}$	$C_{50}H_{53}Cl_2CrI_3N_4O_8S_{12}$	$C_{46}H_{51}Cl_2CrN_5O_8Re_2S_{12}$	$C_{50}H_{53}Br_3CrN_4O_8Re_2S_{12}$
fw	1322.26	1347.54	1585.31	1726.28	1681.94	1886.81
temp/K	293(2)	293(2)	293(2)	293(2)	293(2)	293(2)
radiation, λ/Å	0.71073	0.71073	0.71073	0.71073	0.71073	0.71073
cryst syst	monoclinic	monoclinic	monoclinic	monoclinic	monoclinic	monoclinic
space group	$C2/c$	$C2/c$	$C2/c$	$C2/c$	$C2/c$	$C2/c$
a/Å	33.111(3)	33.087(3)	32.898(3)	32.9459(67)	32.9055(71)	32.9818(23)
b/Å	11.4104(10)	11.5145(10)	11.9855(9)	12.0437(22)	12.1918(22)	12.3182(8)
c/Å	15.9190(16)	16.0359(16)	16.2103(14)	16.3178(33)	16.3414(35)	16.4384(11)
α/deg	90	90	90	90	90	90
β/deg	102.243(3)	102.178(3)	103.822(2)	104.1024(41)	103.4155(62)	103.7556(19)
γ/deg	90	90	90	90	90	90
V/Å^3	5877.7(10)	5971.8(10)	6206.6(9)	6279.6(1)	6376.9(2)	6486.8(6)
Z	4	4	4	4	4	4
d_{calcd}/g cm^{-3}	1.494	1.499	1.697	1.826	1.752	1.932
no. of unique rflns	7653	7467	8140	8108	8355	8129
rflns with $I > 2\sigma(I)$	6208	6107	6873	7130	4806	6796
final R1,[a] wR2[b]	0.0749, 0.2305	0.0762, 0.2251	0.0679, 0.1935	0.0972, 0.2697	0.0837, 0.2228	0.0594, 0.1699

[a] $R1 = \sum||F_o| - |F_c||/\sum|F_o|$. [b] $wR2 = \{\sum[w(F_o^2 - F_c^2)^2]/\sum[w(F_o^2)^2]\}^{1/2}$.

dx.doi.org/10.1021/ic402217c | Inorg. Chem. 2013, 52, 13263−13268

acetonitrile−chlorobenzene mixture gives the weak ferromagnet $[\mathbf{1}][Anion]_2(PhCl)_2(MeCN)$. In the crystal, strong intermolecular interaction is attained by the $\pi-\pi$ stacking of TTF-type ligands, which causes charge and spin delocalization over adjacent molecules. In addition, a strong intramolecular $\pi-d$ interaction of $2J/k_B = -30$ K is also achieved by significant electronic coupling between ethynyl-substituted π-ligands and a transition-metal ion.[13] These inter- and intramolecular interactions result in the strongly connected ferrimagnetic chain structure and a high weak ferromagnetic transition temperature (T_c) of 23 K. Although the results emphasize the usefulness of $[\mathbf{1}]^{n+}$, the origin of the weak ferromagnetism and the significantly different remanent magnetizations for $[BF_4]^-$ and $[ClO_4]^-$ anions remains unclear. In the present paper, we report the solvent- and anion-dependent magnetisms of $[\mathbf{1}][Anion]_2(Solvent1)_2(Solvent2)$ ([Anion] = $[BF_4]^-$, $[ClO_4]^-$, $[ReO_4]^-$, Solvent1 = PhF, PhCl, PhBr, PhI, Solvent2 = MeCN, PhBr, PhI), where the distance between the ferrimagnetic chains is varied. The clear correlation of the magnetism with the crystal structure reveals the origin of the weak ferromagnetism.

EXPERIMENTAL SECTION

Preparation of Compounds. All reagents and solvents were purchased from commercial sources and used without further purification. [1]OTf (OTf = $CF_3SO_3^-$) was prepared according to the procedures in the literature.[12a,14] Black block-shaped crystals of $[\mathbf{1}][Anion]_2(Solvent1)_2(Solvent2)$ were obtained by the galvanostatic oxidation of [1]OTf (14 mg) in a 20 mL solution of $Bu_4N[Anion]$ (30 mg, Anion = $[BF_4]^-$, $[ClO_4]^-$, $[ReO_4]^-$) in a 1.5/1 halogenobenzene (PhF, PhCl, PhBr, PhI)/acetonitrile mixture (0.45 μA, 2−3 weeks). No $[ReO_4]^-$ crystals were obtained from the PhF/acetonitrile solution. Although the $[BF_4]^-$ crystals were obtained from PhBr/acetonitrile and PhI/acetonitrile solutions, and the $[ReO_4]^-$ crystals from PhI/acetonitrile solution, the quality of the crystals were not suitable for this study.

Single-Crystal Structure Determinations. X-ray diffraction measurements were conducted with a four-circle diffractometer (Rigaku AFC-7R) with a Mercury CCD area detector at 293 K using Mo Kα radiation (λ = 0.7107 Å). The structures were solved using direct methods (SIR2004)[15] and then refined by a full-matrix least-squares method (SHELXL-97).[16] A numerical absorption correction was introduced. All non-hydrogen atoms except solvent molecules were refined anisotropically. Hydrogen atoms were placed in their calculated positions and refined using a riding model. The crystallographic data are summarized in Table 1. Full bond lengths and bond angles, atomic coordinates, and complete crystal structure results are presented in the Supporting Information.

Magnetic Measurements. DC magnetic susceptibilities were measured using a SQUID magnetometer (Quantum-Design MPMS-XL) for randomly oriented single crystals encapsulated in aluminum capsules in the temperature range 2−300 K. The paramagnetic contribution of the capsules was calculated on the basis of the weight of the capsules and the standard temperature dependent susceptibility of the capsule. Diamagnetic corrections (in units of 10^{-6} emu mol^{-1}) were estimated from Pascal's constants as −665, −655, −747, −787, −730, and −791 for $[\mathbf{1}][BF_4]_2(PhF)_2(MeCN)$, $[\mathbf{1}][ClO_4]_2(PhF)_2(MeCN)$, $[\mathbf{1}][ClO_4]_2(PhBr)_3$, $[\mathbf{1}][ClO_4]_2(PhI)_3$, $[\mathbf{1}][ReO_4]_2(PhCl)_2(MeCN)$,and $[\mathbf{1}][ReO_4]_2(PhBr)_3$, respectively.

RESULTS AND DISCUSSION

Crystal Structures. All of the obtained crystals are isostructural with the previously reported structures of $[\mathbf{1}][BF_4]_2(PhCl)_2(MeCN)$ and $[\mathbf{1}][ClO_4]_2(PhCl)_2(MeCN)$,[12a] where the asymmetric unit contains half a formula unit. Figure 2 shows the crystal structure of

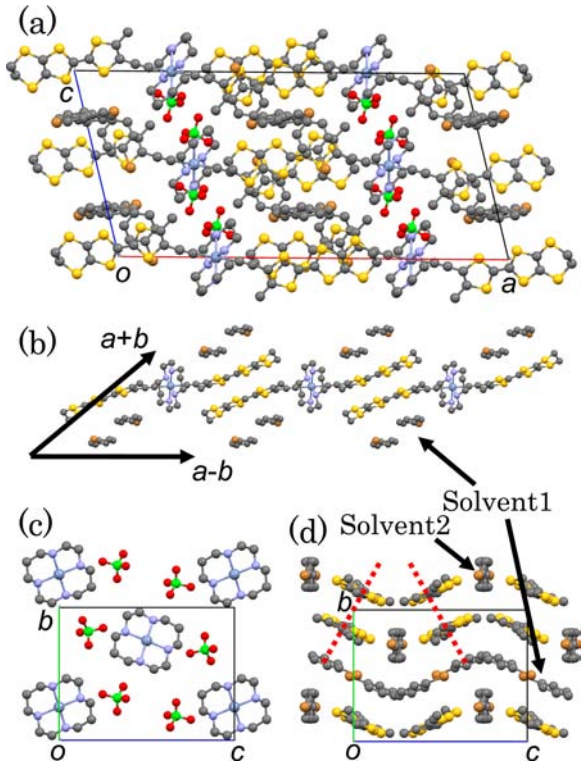

Figure 2. Crystal structures of $[\mathbf{1}][ClO_4]_2(PhBr)_3$: (a) unit cell of the crystal viewed along the b axis; (b) ferrimagnetic chain arrangement of $[\mathbf{1}]^+$ elongated parallel to the $a - b$ direction (neighboring chains are elongated parallel to the $a + b$ direction (not shown)); (c, d) structures of the two different layers viewed along the a axis (dotted red lines emphasize the noncollinear arrangement of the adjacent $(TTF)_2^+$ dimers). Hydrogen atoms are omitted for clarity. Solvent1 and Solvent2 indicate the two crystallographically independent positions of solvent molecules.

$[\mathbf{1}][ClO_4]_2(PhBr)_3$ as a representative of the isostructural crystals. The cation to anion ratio of 1:2 indicates the divalent state of complex $[\mathbf{1}]^{2+}$, where the additional positive charge is due to the oxidation state of the TTF derivatives. Adjacent TTF-type ligands of $[\mathbf{1}]^{2+}$ cations form a $(TTF)_2^+$ dimer, which results in one-dimensional ferrimagnetic chain structures of Cr^{3+}Cyclam ($S = {}^3/_2$) and $(TTF)_2^+$ ($S = {}^1/_2$), as shown in Figure 2b. The chains are elongated parallel to the $a + b$ and $a - b$ directions. The crystal structure is characterized by the two types of layers stacked alternately along the a axis. The first layer consists of Cr^{3+}Cyclam units and anions, while the second layer consists of $(TTF)_2^+$ radical cations and solvent molecules. In the first layer, each Cr^{3+}Cyclam unit is separated by six adjacent anions (Figure 2c). There are two slightly short X···HN (X = F for $[BF_4]^-$ salts and X = O for $[ClO_4]^-$ and $[ReO_4]^-$ salts) contacts between an anion and adjacent Cyclam units. For instance, F···HN contacts of 3.041(5) and 3.071(5) Å are found in $[\mathbf{1}][BF_4]_2(PhF)_2(MeCN)$. The weak hydrogen bonds at the contacts probably play an important role in preventing the rotation of the anions. In the second layer, there are two types of solvent molecules, referred to as Solvent1 and Solvent2, as shown in Figure 2d. The position of Solvent1 is always occupied by halogenobenzene molecules that isolate the $(TTF)_2^+$ dimers in the b direction and form zigzag chains elongated parallel to the c axis; therefore, larger halogenobenzene molecules cause a longer c axis and a larger space at the position of Solvent2. When a larger halogenobenzene such

dx.doi.org/10.1021/ic402217c | Inorg. Chem. 2013, 52, 13263−13268

as PhBr or PhI is used as a solvent, the position of Solvent2 is also occupied by a halogenobenzene molecule. However, if a smaller halogenobenzene such as PhF or PhCl is used, then the position is occupied by an acetonitrile molecule because the space is too small to be occupied by a halogenobenzene. In either case, the orientation of Solvent2 is disordered.

From a magnetic point of view, there are two important structural parameters: the overlap of TTF-type ligands, which results in ferrimagnetic chains of $[\mathbf{1}]^{2+}$, and the shortest sulfur−sulfur distance (d_{S-S}) between adjacent $(TTF)_2^+$ dimers, which corresponds to an interchain interaction.[12a] The observed crystal structures indicate that neither the substitution of an anion nor that of a halogenobenzene affects the overlap of TTF-type ligands. The insensitivity of the overlap is a natural consequence of the anions and solvent molecules being placed outside of a ferrimagnetic chain, so that they do not affect the intrachain structure. In contrast to the intrachain structure, the interchain distance is significantly dependent on the substitutions; the values of d_{S-S} are summarized in Table 2. Anions

Table 2. Values of d_{S-S}/Å

	halogenobenzene			
anion	PhF	PhCl	PhBr	PhI
$[BF_4]^-$	3.960(2)	3.827(2)[12a]	low quality	low quality
$[ClO_4]^-$	3.997(2)	3.854(2)[12a]	3.814(1)	3.803(2)
$[ReO_4]^-$	no crystal	3.910(4)	3.899(2)	low quality

are placed at the midpoint of Cr^{3+}Cyclam units; therefore, larger anions extend the interchain distances in the *bc* plane, which results in longer d_{S-S} values. For example, the d_{S-S} values of $[\mathbf{1}][Anion]_2(PhCl)_2(MeCN)$ are 3.827(2), 3.854(2), and 3.910(4) Å for [Anion] = $[BF_4]^-$ (smallest anion), $[ClO_4]^-$, $[ReO_4]^-$ (largest anion), respectively. The d_{S-S} value is also affected by the halogenobenzene substitution, but in the opposite direction; i.e., a larger halogenobenzene causes a shorter d_{S-S} value. For instance, the d_{S-S} values of $[\mathbf{1}][ClO_4]_2$(Solvent1)(Solvent2) are 3.997(2), 3.854(2), 3.814(1), and 3.803(2) Å for Solvent1 = PhF, PhCl, PhBr, PhI, respectively, while the *c* axis of the crystal increases monotonically from 16.0359(16) to 16.3178(33) Å. This unexpected relation can be explained by the rotation of $[\mathbf{1}]^{2+}$. To fill surplus spaces in the *c* direction caused by larger halogenobenzene molecules, the $[\mathbf{1}]^{2+}$ molecules are slightly rotated in the *ab* plane, as represented by an increase in the β angle, and the rotation accidentally shortens the interdimer distance.

Magnetic Properties. The magnetic susceptibilities χ of six new materials are indistinguishable from the previous data for $[\mathbf{1}][BF_4]_2(PhCl)_2(MeCN)$ and $[\mathbf{1}][ClO_4]_2(PhCl)_2(MeCN)$ in the high-temperature region. The best fit of $1/\chi$ in the temperature range $100 \leq T \leq 300$ K gives the Curie constants C = 2.37, 2.26, 2.32, 2.29, 2.37, and 2.38 emu K mol^{-1} and Weiss temperatures Θ = −41, −39, −40, −42, −43, and −43 K for $[\mathbf{1}][BF_4]_2(PhF)_2(MeCN)$, $[\mathbf{1}][ClO_4]_2(PhF)_2(MeCN)$, $[\mathbf{1}][ReO_4]_2(PhCl)_2(MeCN)$, $[\mathbf{1}][ClO_4]_2(PhBr)_3$, $[\mathbf{1}][ReO_4]_2(PhBr)_3$, and $[\mathbf{1}][ClO_4]_2(PhI)_3$, respectively (see the Supporting Information, Figure S1). The values of C are in approximate agreement with the sum of the spin-only value of $S = {}^3/_2$ (1.875 emu K/mol) and ${}^1/_2$ (0.375 emu K/mol). The almost identical values of Θ are a natural consequence of the same intrachain structure, because the Weiss temperatures of these compounds are governed mainly by the strong intrachain interaction, while the weak interchain interaction is negligible in the high-temperature region.

Figure 3 shows the temperature dependencies of the χT values, which gradually decreases with the temperature,

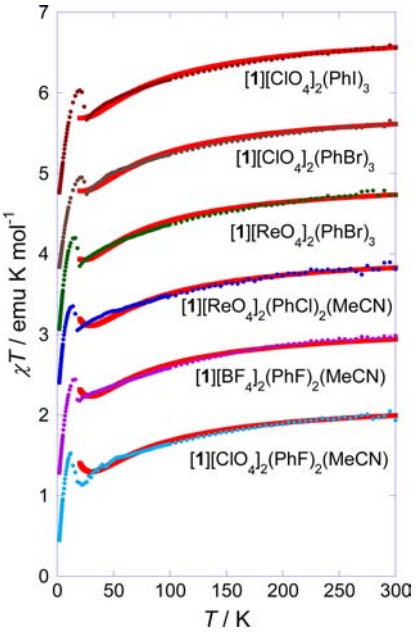

Figure 3. Temperature dependence of χT for the nonoriented samples. Data for $[\mathbf{1}][BF_4]_2(PhF)_2(MeCN)$, $[\mathbf{1}][ReO_4]_2(PhCl)_2(MeCN)$, $[\mathbf{1}][ReO_4]_2(PhBr)_3$, $[\mathbf{1}][ClO_4]_2(PhBr)_3$, and $[\mathbf{1}][ClO_4]_2(PhI)_3$ are vertically shifted up by 0.9, 1.8, 2.7, 3.6, and 4.5, respectively, for clarity. The red solid lines are fitting curves using eq 2 with fitting parameters of $2J/k_B = -30$ K and $\alpha = -1.2$ for $[\mathbf{1}][ClO_4]_2(PhF)_2(MeCN)$ and $[\mathbf{1}][BF_4]_2(PhF)_2(MeCN)$, $2J/k_B = -30$ K and $\alpha = -1.4$ for $[\mathbf{1}][ReO_4]_2(PhCl)_2(MeCN)$, $2J/k_B = -28$ K and $\alpha = -1.8$ for $[\mathbf{1}][ReO_4]_2(PhBr)_3$, $2J/k_B = -29$ K and $\alpha = -2.2$ for $[\mathbf{1}][ClO_4]_2(PhBr)_3$, and $2J/k_B = -30$ K and $\alpha = -2.3$ for $[\mathbf{1}][ClO_4]_2(PhI)_3$ (see text).

followed by small jumps due to the weak ferromagnetic transition, as discussed later. To estimate the strengths of the intra- and interchain interactions, the following analytical expression for the χT value of weakly interacting $[{}^1/_2{-}{}^3/_2]$ ferrimagnetic chains[17] is used, where the interchain interaction is treated in the mean-field approximation:

$$\chi T = \chi_{1D} T \left(1 + \frac{\alpha \chi_{1D}}{1 - \alpha \chi_{1D}} \right) \tag{2}$$

$$\chi_{1D} = \frac{1}{T} \left\{ 0.5756 \left(\frac{|2J|}{k_B T} \right)^{1.80} + 2.250 \exp\left(-0.882 \frac{|2J|}{k_B T} \right) \right\} \tag{3}$$

$$\alpha = \frac{2zJ'}{g^2 \mu_B{}^2 N} \tag{4}$$

where χ_{1D}, k_B, g, μ_B, N, J, z, and J' are the susceptibility of the isolated $[{}^1/_2{-}{}^3/_2]$ ferrimagnetic chain, the Boltzmann constant, g value, the Bohr magneton, the Avogadro constant, the intrachain exchange interaction defined in eq 1, the number of interchain interaction paths, and the strength of the effective interchain interaction in the mean field approximation, respectively. The best fit of the χT values in the temperature

dx.doi.org/10.1021/ic402217c | Inorg. Chem. 2013, 52, 13263−13268

range from 40 to 300 K gives an intrachain interaction almost identical with that of $2J/k_B = -29 \pm 1$ K, which is consistent with the Weiss temperature. In contrast, the interchain interaction is clearly dependent on d_{S-S}. The fitting parameter $-\alpha$, which is proportional to the strength of the interchain interaction shown in eq 4, increases monotonically from 1.2 to 2.3 as d_{S-S} decreases from 3.997(2) to 3.803(2) Å (Supporting Information, Figure S2). The observed relation between d_{S-S} and α is an inevitable result, because a shorter interchain distance typically causes a stronger interchain interaction.

Although all of the materials exhibit weak ferromagnetism at low temperature, as previously reported in the isostructural systems, T_c and the remanent magnetization values (M_{rem}) are quite different from each other. Figure 4 shows the field-cooled

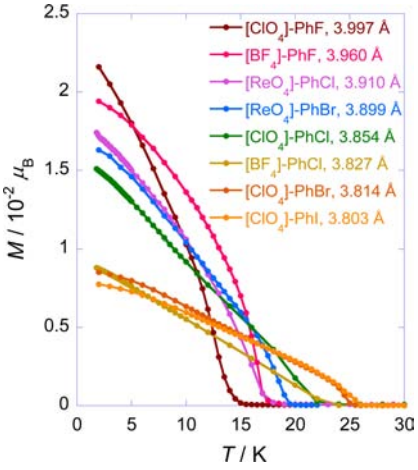

Figure 4. Field-cooled magnetization (1 mT) of $[\mathbf{1}][ClO_4]_2(PhF)_2(MeCN)$ (dark brown), $[\mathbf{1}][BF_4]_2(PhF)_2(MeCN)$ (red), $[\mathbf{1}][ReO_4]_2(PhCl)_2(MeCN)$ (purple), $[\mathbf{1}][ReO_4]_2(PhBr)_3$ (blue), $[\mathbf{1}][ClO_4]_2(PhCl)_2(MeCN)$ (green),[12a] $[\mathbf{1}][BF_4]_2(PhCl)_2(MeCN)$ (olive),[12a] $[\mathbf{1}][ClO_4]_2(PhBr)_3$ (brown), and $[\mathbf{1}][ClO_4]_2(PhI)_3$ (orange). The number in the legend denotes the d_{S-S} value of the material.

(FC) magnetizations with a magnetic field of 1 mT, and Figure 5 shows plots of T_c, M_{rem} at 2 K, and the coercive force (H_c) vs d_{S-S}. T_c decreases from 26.0 to 14.5 K as d_{S-S} increases from 3.803(2) to 3.997(2) Å, which is reasonable because a longer interchain distance usually indicates a weaker interchain interaction and lower transition temperature. In contrast to the case for T_c, the value of M_{rem} at 2 K rapidly increases from 0.0079 to 0.0215 μ_B as the interchain distance increases.

The results indicates that the interchain interaction suppresses the canted spin alignment, and similar phenomena are often observed when pressure is applied to a weak ferromagnet with single-ion anisotropy.[18] In the present crystals, there is no inversion center between the neighboring $[\mathbf{1}]^{2+}$ cations of the adjacent ferrimagnetic chains. For example, the alignment of contiguous $(TTF)_2^+$ dimers is noncollinear, as shown in Figure 2d, where the single-ion anisotropy and Dzyaloshinsky–Moriya (D-M) interaction can cause a canted spin alignment and nonvanishing net magnetic moments. In the case where the weak ferromagnetism is caused by single-ion anisotropy, an interchain antiferromagnetic (AF) interaction merely weakens the weak ferromagnetism because the AF interaction prefers a noncanted antiparallel spin alignment. In contrast, if the weak ferromagnetism is caused by a D-M interaction, then a stronger interchain AF interaction also

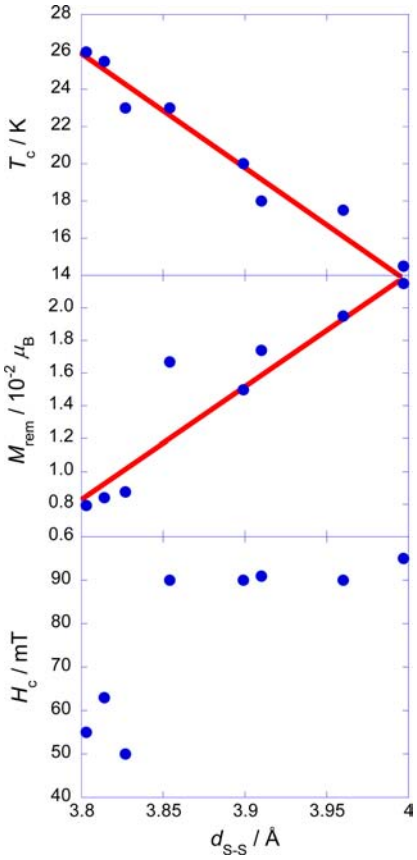

Figure 5. T_c (top), M_{rem} at 2 K (middle), and H_c (bottom) at 2 K as a function of d_{S-S}. T_c is determined as the temperature at the point where the FC and zero-field cooled magnetization start to split (also see Supporting Information, Figure S3). The solid red lines are guides for eyes.

causes a stronger D-M interaction, which enhances the weak ferromagnetism; i.e., the weak ferromagnetism is more insensitive to an increase in the interchain AF interaction. Hence, the observed large d_{S-S} dependence of M_{rem} indicates that the origin of the weak ferromagnetism is principally the single-ion anisotropy of $[\mathbf{1}]^{2+}$.

At the end of this section, we briefly mention the change of H_c. The values of H_c seems to be classified into two groups: large H_c values of ca. 90 mT in the region of $d_{S-S} > 3.854(2)$ Å and smaller H_c values of ca. 55 mT for $d_{S-S} < 3.827(2)$ Å, as shown in Figure 5. The result suggests that some change occurs at around $d_{S-S} = 3.84$ Å. The existence of the change is also supported by the d_{S-S} dependencies of M_{rem} and FC magnetization that also have a gap at the point as shown in Figures 4 and 5. However, the reason for the observed gap remains unclear at the present time.

CONCLUSION

A series of new weak ferromagnets containing a chromium–acetylide–TTF type complex, $[\mathbf{1}][Anion]_2(Solvent1)_2(Solvent2)$, were reported. The crystals are isostructural and are characterized by a ferrimagnetic chain of $[\mathbf{1}]^{2+}$. The shortest interchain distance can be modified by solvent and anion substitution in the range $d_{S-S} = 3.803(2)$–3.997(2) Å, where T_c and M_{rem} at 2 K also vary from 26.0 to 14.5 K and 0.0079 to 0.0215 μ_B, respectively. The higher T_c value at shorter d_{S-S} is due to a stronger interchain AF

dx.doi.org/10.1021/ic402217c | Inorg. Chem. 2013, 52, 13263–13268

interaction, which also forces an antiparallel spin arrangement of adjacent ferrimagnetic chains, which results in the smaller M_{rem}. The results strongly indicate that the origin of the weak ferromagnetism is not D-M interaction but rather single-ion anisotropy.

■ ASSOCIATED CONTENT

Supporting Information

Figures giving $1/\chi$ vs T plots, d_{S-S} dependencies of the fitting parameters of intrachain interaction $2J/k_B$ and α ($\propto$ effective interchain interaction), magnetization curves at 2 K, and FC and zero-field cooled magnetizations and CIF files giving X-ray crystallographic data. This material is available free of charge via the Internet at http://pubs.acs.org.

■ AUTHOR INFORMATION

Corresponding Author

*J.N.: e-mail, jun-ichi.nishijo@meisei-u.ac.jp; tel and fax, +81-42-591-7542.

Notes

The authors declare no competing financial interest.

■ REFERENCES

(1) (a) Gibson, V. C.; Redshaw, C.; Solan, G. A. *Chem. Rev.* **2007**, *107*, 1745−1776. (b) Luca, O. R.; Crabtree, R. H. *Chem. Soc. Rev.* **2013**, *42*, 1440−1459. (c) Praneeth, V. K. K.; Ringenberg, M. R.; Ward, T. R. *Angew. Chem., Int. Ed.* **2012**, *51*, 10228−10234. (d) Munhá, R. F.; Zarkesh, R. A.; Heyduk, A. F. *Dalton Trans.* **2013**, *42*, 3751−3766.

(2) Arounaguiri, S.; Maiya, B. G. *Inorg. Chem.* **1999**, *38*, 842−843.

(3) (a) Lindsay, S.; Lo, S. K.; Maguire, O. R.; Bill, E.; Probert, M. R.; Sproules, S.; Hess, C. R. *Inorg. Chem.* **2013**, *52*, 898−909. (b) Yu, M.; Beyers, R. J.; Gorden, J. D.; Cross, J. N.; Goldsmith, C. R. *Inorg. Chem.* **2012**, *51*, 9153−9155. (c) Das, A.; Scherer, M.; Chowdhury, A. D.; Mobin, S. M.; Kaim, W.; Lahiri, G. K. *Inorg. Chem.* **2012**, *51*, 1675−1684.

(4) (a) Lorcy, D.; Bellec, N.; Fourmigué, M.; Avarvari, N. *Coord. Chem. Rev.* **2009**, *253*, 1398−1438. (b) Rabaça, S.; Almeida, M. *Coord. Chem. Rev.* **2010**, *254*, 1493−1508. (c) Riobé, F.; Avarvari, N. *Coord. Chem. Rev.* **2010**, *254*, 1523−1533. (d) Justaud, F.; Gendron, F.; Ogyu, Y.; Kumamoto, Y.; Miyazaki, A.; Ouahab, L.; Costuas, K.; Halet, J.-F.; Lapinte, C. *Chem. Eur. J.* **2013**, *19*, 5742−5757. (e) Vacher, A.; Barrière, F.; Camerel, F.; Bergamini, J.-F.; Roisnel, T.; Lorcy, D. *Dalton Trans.* **2013**, *42*, 383−394.

(5) Yamada, J.-I.; Sugimoto, T. *TTF Chemistry: Fundamentals And Applications Of Tetrathiafulvalene*; Springer: Berlin, 2004.

(6) Náfrádi, B.; Olariu, A.; Forró, L.; Mézière, C.; Batail, P.; Jánossy, A. *Phys. Rev. B* **2010**, *81*, 224438.

(7) (a) Bivaud, S.; Balandier, J.-Y.; Chas, M.; Allain, M.; Goeb, S.; Sallé, M. *J. Am. Chem. Soc.* **2012**, *134*, 11968−11970. (b) Qin, Y.-R.; Zhu, Q.-Y.; Huo, L.-B.; Shi, Z.; Bian, G.-Q.; Dai, J. *Inorg. Chem.* **2010**, *49*, 7372−7381.

(8) Tsunashima, R.; Matsumoto, T.; Hoshino, N.; Niiho, W.; Kimura, M.; Kondo, K.; Suyama, Y.; Nishioka, Y.; Kawamata, J.; Noro, S.; Nakamura, T.; Akutagawa, T.; Ishiguro, K. *Dalton Trans.* **2012**, *41*, 10060−10064.

(9) (a) Keniley, L. K., Jr.; Dupont, N.; Ray, L.; Kovnir, K.; Hoyt, J. M.; Hauser, A.; Shatruk, M. *Inorg. Chem.* **2013**, *52*, 8040−8052. (b) Pointillart, F.; Bpurdolle, A.; Cauchy, T.; Maury, O.; Gal, Y. L.; Golhen, S.; Cador, O.; Ouahab, L. *Inorg. Chem.* **2011**, *51*, 978−984.

(10) (a) Pointillart, F.; Klementieva, S.; Kuropatov, V.; Gal, Y. L.; Golhen, S.; Cador, O.; Cherkasov, V.; Ouahab, L. *Chem. Commun.* **2012**, *48*, 714−716. (b) Kolotilov, S. V.; Cador, O.; Pointillart, F.; Golhen, S.; Gal, Y. L.; Gavrilenko, K. S.; Ouahab, L. *J. Mater. Chem.* **2010**, *20*, 9505−9514. (c) Yokota, S.; Tsujimoto, K.; Hayashi, S.; Pointillart, F.; Ouahab, L.; Fujiwara, H. *Inorg. Chem.* **2013**, *52*, 6543−6550.

(11) (a) Shatruk, M.; Ray, L. *Dalton Trans.* **2010**, *39*, 11105−11121. (b) Pointillart, F.; Guennic, B. L.; Cauchy, T.; Golhen, S.; Cador, O.; Maury, O.; Ouahab, L. *Inorg. Chem.* **2013**, *52*, 5978−5990. (c) Dupont, N.; Ran, Y.-F.; Liu, S.-X.; Grilj, J.; Vauthey, E.; Decurtins, S.; Hauser, A. *Inorg. Chem.* **2013**, *52*, 306−312. (d) Pointillart, F.; Golhen, S.; Cador, O.; Ouahab, L. *Dalton Trans.* **2013**, *42*, 1949−1960.

(12) (a) Nishijo, J.; Judai, K.; Nishi, N. *Inorg. Chem.* **2011**, *50*, 3464−3470. (b) Nishijo, J. *Polyhedron* **2013**, DOI: 10.1016/j.poly.2013.01.035.

(13) (a) Vacher, A.; Barrière, F.; Roisnel, T.; Piekara-Sady, L.; Lorcy, D. *Organometallics* **2011**, *30*, 3570−3578. (b) Cai, X.-M.; Zhang, X.-Y.; Savchenko, J.; Cao, Z.; Ren, T.; Zuo, J.-L. *Organometallics* **2013**, *31*, 8591−8597. (c) Miyazaki, A.; Ogyu, Y.; Justaud, F.; Ouahab, L.; Cauchy, T.; Halet, J.-F.; Lapinte, C. *Organometallics* **2010**, *29*, 4628−4638. (d) Vacher, A.; Barrière, F.; Roisnel, T.; Lorcy, D. *Chem. Commun.* **2009**, 7200−7202. (e) Cao, Z.; Forrest, W. P.; Gao, Y.; Ranwick, P. E.; Ren, T. *Organometallics* **2012**, *31*, 6199−6206. (f) Sun, C.; Thakker, P. U.; Khulordava, L.; Tobben, D. J.; Greenstein, S. M.; Grisenti, D. L.; Kantor, A. G.; Wagenknecht, P. S. *Inorg. Chem.* **2012**, *51*, 10477−10479.

(14) (a) John, D. E.; Moore, A. J.; Bryce, M. R.; Batsanov, A. S.; Leech, M. A.; Howard, A. K. *J. Mater. Chem.* **2000**, *10*, 1273−1279. (b) Bakac, A.; Espenson, J. H. *Inorg. Chem.* **1992**, *31*, 1108−1110. (c) Wright-Garcia, K.; Basinger, J.; Williams, S.; Hu, C.; Wagenknecht, P. S. *Inorg. Chem.* **2003**, *42*, 4885−4890. (d) Grisenti, D. L.; Thomas, W. W.; Turlington, C. R.; Newsom, M. D.; Priedemann, C. J.; VanDerveer, D. G.; Wagenknecht, P. S. *Inorg. Chem.* **2008**, *47*, 11452−11454.

(15) Burla, M. C.; Caliandro, R.; Camalli, M.; Carrozzini, B.; Cascarano, G. L.; De Caro, L.; Giacovazzo, C.; Polidori, G.; Spagna, R. *J. Appl. Crystallogr.* **2005**, *38*, 381−388.

(16) Sheldrick, G. M. *Acta Crystallogr., Sect. A* **2008**, *64*, 112−122.

(17) (a) Nishijo, J.; Judai, K.; Numao, S.; Nishi, N. *Inorg. Chem.* **2009**, *48*, 9402−9408. (b) Miller, J. S.; Drillon, M. *Magnetism: Molecules to Materials*; Wiley-VCH: Weinheim, Germany, 2001; Vol. *I*. It should be noted that the definition of exchange interaction "*J*" in the reference is equal to "2*J*" in this report.

(18) (a) DaSilva, J. G.; Miller, J. S. *Inorg. Chem.* **2013**, *52*, 1418−1423. (b) Kudo, S.; Miyazaki, A.; Enoki, T.; Golhen, S.; Ouahab, L.; Toita, T.; Yamada, J. *Inorg. Chem.* **2006**, *45*, 3718−3725.